PROCEEDINGS, 42nd Workshop on Geothermal Reservoir Engineering
Stanford University, Stanford, California, February 13-15, 2017
SGP-TR-212

Investigation of Physical Mechanisms that Influence Injection-Induced Earthquake Sequence Statistics

Lauren S. Abrahams[1], Jack H. Norbeck[2,3] and Roland N. Horne[2]

[1]University of Wisconsin - Madison, Madison, Wisconsin, USA, 53715

[2]Department of Energy Resources Engineering, Stanford University, Stanford, California, USA, 94305

[3]Earthquake Science Center, United States Geological Survey, Menlo Park, California, USA, 94025

labrahams@wisc.edu

Keywords: earthquake sequence, dynamic friction, injection rate

ABSTRACT

In this work, numerical modeling was used to investigate how fluid injection influences the statistical properties of injection-induced earthquake sequences. The numerical model calculated the coupled processes of fluid flow in aquifers and faults, mechanical deformation, and quasidynamic earthquake rupture. Injection-induced earthquake sequences were simulated by modeling fluid injection into a porous aquifer that contained many faults, which were represented explicitly within an embedded fracture modeling framework. The earthquake rupture process was modeled using a rate-and-state constitutive model of fault friction. The Oklahoma fault map database provided by Holland (2015) was used to develop distributions of two-dimensional fault structures for four synthetic study areas. A sensitivity study was performed to characterize the relationship between the statistical properties of earthquake sequences and both geological and operational model parameters.

Sensitivity studies were performed to assess the effect of both dynamic friction and variability of injection rate over time on statistics of simulated earthquake sequences. It was found that at lower dynamic friction, earthquake nucleation occurred with less injected volume, the maximum magnitude increased, and total number of earthquakes increased. The effects of a variable injection operational schedule were investigated by comparing constant-rate injection to a scenario where the well cycled between periods of injection and shut-in on a monthly basis. This study was performed using fixed pressure and no-flow boundary conditions for each of the four study areas. For the fixed pressure boundary cases there was an increase in seismicity when fluid was cycling monthly, likely due to higher pressures that occurred near the pumping site. For the no-flow boundary condition, the earthquake sequences were nearly identical in terms of the earthquake magnitude distribution, event timing, and total number of events.

The Oklahoma Corporation Commission has placed mandates on disposal wells that are thought to be linked to significant earthquake events (Baker, 2016). However, there still is not a clear procedure for how to most efficiently manage injection well operation in order to reduce the seismic hazard. Therefore, the use of a numerical modeling system is fundamental in order to create a better understanding of induced seismicity and help shape impactful regulation.

1. INTRODUCTION

In 2014, the rate of occurrence of earthquakes in Oklahoma with magnitude 3 and larger exceeded that of California (McGarr et al., 2015). This increase in seismicity has been associated with the disposal of large volumes of water through injection into deep subsurface aquifers (Ellsworth, 2013; McGarr, 2014; Walsh and Zoback, 2015). Geothermal development risks the loss of public acceptance if induced seismicity becomes a problem (Majer, 2007), so understanding induced seismicity is essential to ensure the orderly expansion of geothermal energy utilization. Oklahoma provides some very comprehensive site observations of induced earthquakes, and hence is a useful case study to develop our understanding of the phenomenon. The 2014 USGS National Seismic Hazard Model did not incorporate induced seismicity; it was unforeseen that induced seismicity would have such a significant risk. In fact, some areas were three times more hazardous than the model had predicted (Petersen et al., 2016). The 2016 seismic hazard model incorporated induced seismicity because it had a substantial influence on the seismicity in the central and eastern United States (Petersen et al., 2016). In the National Seismic Hazard Model, the probability of experiencing a given-magnitude earthquake is calculated using the frequency-magnitude statistics at each location based on observational data. Furthermore, the earthquake statistics are assumed to remain stationary over the forecast duration (Peterson et al., 2016). Further research is warranted to fully understand how injection influences the magnitude of these earthquakes, the timing of these earthquakes, and the total number of events.

Many companies, including oil, gas, and geothermal, use a large amount of water to extract resources from the ground. To dispose of this water it is pumped deep into the subsurface to keep from contaminating drinking water (Shammas et al., 2016). When this water is pumped into the subsurface it increases the pore pressure, causing effective stress to decrease (Ellsworth, 2013). Fault stability diminishes with decreasing effective stress, which can promote earthquake triggering.

Increase in induced earthquakes has caused Oklahoma to take action. After large magnitude earthquakes started occurring, the Oklahoma Corporation Commission (OCC) mandated reduction in the volume of wastewater disposed with the objective to decrease the seismicity in the area (Baker, 2016). Specifically, in 2015, the OCC required over 700 Underground Injection Control (UIC) Class-II

injection wells that were completed in the Arbuckle formation to reduce injection to 60% of the 2014 levels, which was expected to achieve a total reduction of approximately 800,000 bbl/day (Baker, 2016). Because induced seismicity in the area is related directly with the manner in which wastewater disposal is carried out, changes in the operational conditions of injection wells throughout the state should be considered in the seismic hazard analysis.

In this work, numerical modeling was used to investigate the manner in which fluid injection influences the statistical properties of injection-induced earthquake sequences. The goal of the project was to use a numerical model to understand how physical controls affect the statistical properties that inform seismic hazard analyses. The physical controls tested were dynamic friction and injection rate. The statistical properties evaluated were the Gutenberg-Richter a-value (seismicity rate) and b-value (frequency-magnitude scaling factor) to understand the frequency-magnitude distribution, event timing, and total number of earthquakes.

This paper is organized as follows. In Section 2, we present the methodology used to perform our numerical experiments. In Sections 3 and 4, we present the modeling results for the dynamic friction experiment (Case 1) and injection rate variability experiment (Case 2), respectively. A discussion and further analysis of our results is presented in Section 5. Finally, several concluding remarks are presented in Section 6.

2. METHODS

In this work, a numerical modeling system was used to understand how physical controls affected statistical properties of earthquake sequences. To perform this analysis the numerical modeling software CFRAC was used on four synthetic study areas that approximately exhibited the Oklahoma fault structure. We performed two studies to assess the sensitivity of the earthquake statistics to different model parameters. In Case 1, we varied the value of fault dynamic friction, which is a geological parameter. The dynamic friction experiment was tested using a no flow boundary condition. In Case 2, we investigated the variability of injection rate over time, which is an operational parameter. Case 2 was performed using no flow boundary conditions (Case 2A) and fixed pressure boundary conditions (Case 2B).

2.1 Numerical Modeling System CFRAC

The numerical modeling software used for this project was Complex Fracture ReseArch Code (CFRAC). CFRAC was written originally by McClure (2012) and further modified as in Norbeck (2016). Detailed descriptions of the numerical formulations used in CFRAC are provided by Norbeck et al. (2016), Norbeck and Horne (2016), and Norbeck (2016). CFRAC is a fractured reservoir numerical model that calculates the coupled processes of fluid flow in porous media and fracture mechanics. The CFRAC model is capable of solving the fully-coupled system of equations that describe fluid flow (finite volume method), fault deformation (displacement discontinuity method), and earthquake rupture (rate-and-state friction). By using a rate-and-state friction description of the earthquake nucleation, rupture, and arrest processes, we were able to perform physics-based forward models of injection-induced earthquake sequences on multiple faults that existed within the model domain. Hence, we investigated how different geological and operational parameters effected the earthquake frequency-magnitude distribution, event timing, and total number of events.

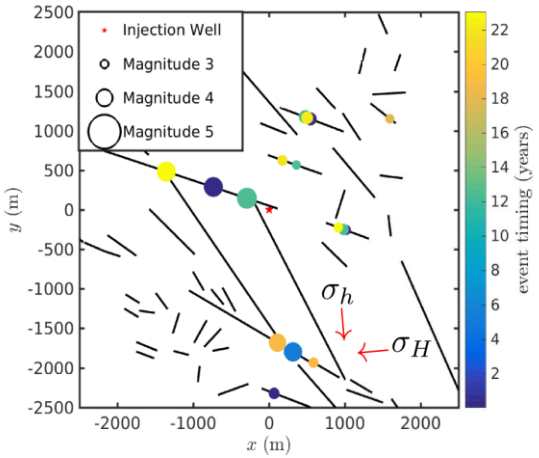

Figure 1: CFRAC outputs the data in a written form, which then can be represented in a figure. The state of stress was assumed to by strike- slip with maximum horizontal stress oriented N85°E. Injection is occurring at the star at the center of the model. The lines represent the faults generated for the model. The colored circles represent the triggered earthquake; the size of the circle corresponds to magnitude and color corresponds to event timing.

2.2 Initial Conditions

The goal of our numerical experiments was to understand Oklahoma seismicity; therefore, an attempt was made to create conditions to best represent the state. For this experiment the Oklahoma fault map database (Holland, 2015) was used to develop distributions of two-dimensional fault structures for four synthetic study areas. The state of stress was assumed to by strike-slip with maximum horizontal stress oriented N85°E and the stress magnitudes at depth were chosen to reflect that of central Oklahoma (Walsh and Zoback, 2016). For the injection rate experiment no flow boundary conditions were used, for the injection rate variability experiment both no flow boundary conditions and fixed pressure boundary conditions were assessed.

2.2.1 Model Properties

In the dynamic friction experiment (Case 1), four rate and state friction b-values were tested (0.011, 0.014, 0.018, and 0.022). The rate-and-state friction b-values corresponded to the dynamic friction values of 0.6270, 0.5579, 0.4658, and 0.3737. Pumping rate was set to a constant 9kg/s (4891 bbl/d) throughout the entire experiment that ran for 25 years.

In the injection rate variability experiment (Case 2), two different injection schedules were compared. The first pumping schedule was a constant 9 kg/s (4891 bbl/d) injection rate. The second pumping schedule injected at a rate of 18kg/s (9782 bbl/d) and cycled between periods of injection and shut-in on a monthly basis. The cumulative volume of fluid injected was the same in both simulations. Dynamic friction was constant at 0.5579 (rate-and-state friction b-values 0.014).

The relevant model parameters for the simulations are given in Table 1. These parameters were held constant throughout both experiments.

Table 1: Model parameters used in the CFRAC models for both dynamic friction experiment (Case 1) and injection rate variability experiment (Case 2)

Parameter	Symbol	Value	Unit
Poisson's Ratio	υ	0.25	-
Initial Fluid Pressure	P_{int}	45	MPa
Stress for hydraulic aperture	e_0	100	MPa
Stress for void aperture	E_0	100	MPa
Rate-and-State (a-value)	a	0.01	-
Rate-and-State Friction (dc-value)	dc	2.00E-03	m
Permeability (x, y and z axis)	κ	1.00E-13	m^2
Remote Compressive Stress x-axis	σ_{xx}	149.43	MPa
Remote Compressive Stress y-axis	σ_{yy}	75.57	MPa
Remote Shear Stress	σ_{xy}	6.52	MPa
Shear Modulus	G	15000	MPa

2.2.2 Fault Distribution

Four synthetic study areas were designed to represent the Oklahoma fault structure. Figure 2 shows the Oklahoma fault map database provided by Holland (2015). The Oklahoma fault maps represents known faults based on surface expressions or seismic reflection data (typically focused on the sedimentary lithological units). In Figure 2, the red boxes show the regions that were used to generate the four synthetic study areas. Figure 3 shows how the true Oklahoma fault structure was then converted into the four synthetic study areas. These four synthetic study areas were scaled to have a domain size of 5 km by 5 km with the aspect ratio remaining constant. In the simulations, fluid injection occurred at the center of each study area.

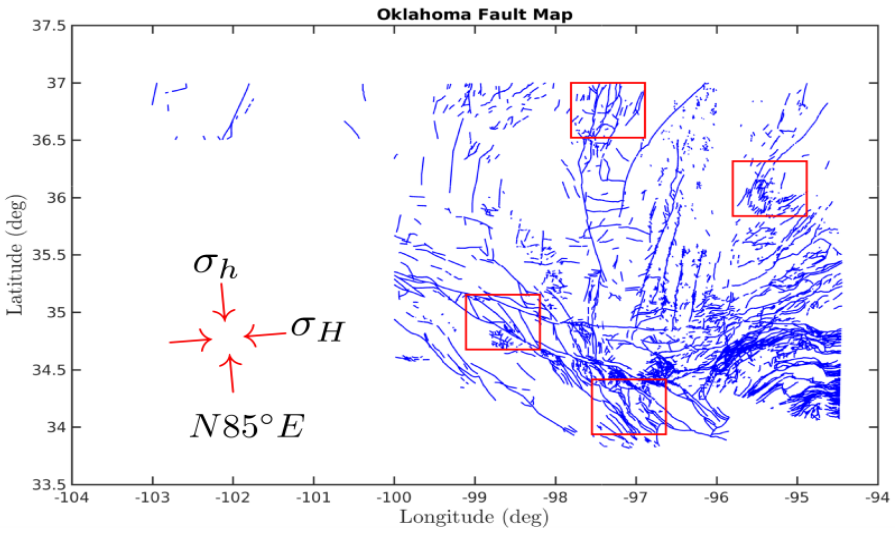

Figure 2: The Oklahoma fault map database was used to develop distributions of two-dimensional fault structures for four synthetic study areas (Holland, 2015). Red boxes indicated faults used to create synthetic study areas. The state of stress was assumed to by strike- slip with maximum horizontal stress oriented N85°E.

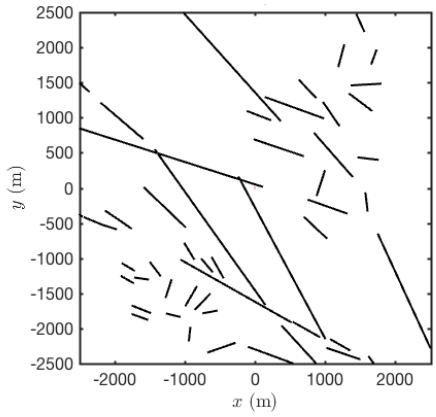

Study Area 1: West
Total number of fractures: 52

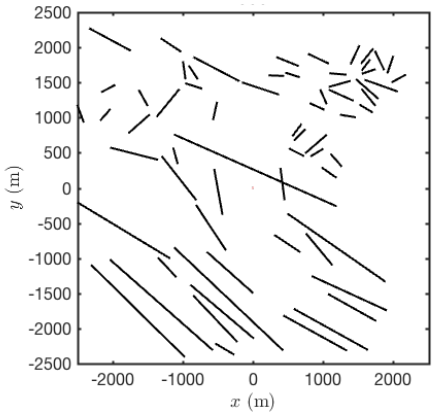

Study Area 2: South
Total number of fractures: 66

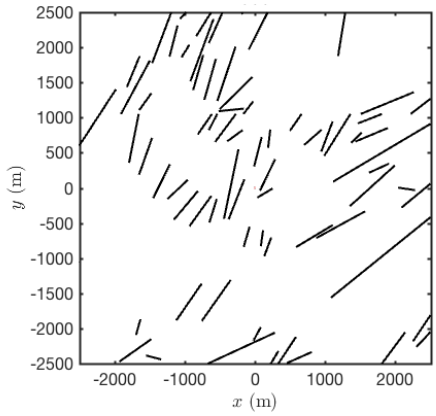

Study Area 3: East
Total number of fractures: 73

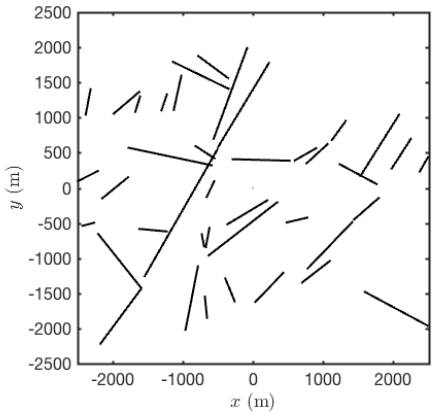

Study Area 4: North
Total number of fractures: 41

Figure 3: Four synthetic study areas used in the CFRAC model that approximated the Oklahoma fault structure

2.2.3 Boundary Conditions

In the CFRAC simulation water injection occurred at the center of the system and flowed through the aquifer and faults outward towards the boundary of the 5000 m by 5000 m study area. We considered both no flow and constant pressure boundary conditions. For the no flow boundary conditions the pressure gradient moved outward toward the boundary and continuously rose as if the outer edges are impermeable trapping the fluid mass in the area. The pressure gradient across the boundary is zero. For the fixed pressure boundary the pressure gradient at the boundary can change, but, outer edge maintained a constant pressure of 45 MPa. For the dynamic friction experiment (Case 1) the test was run with a no flow boundary conditions. For the injection rate variability experiment the test was run with both no flow boundary (Case 2A) and fixed pressure boundaries (Case 2B).

3. EXPERIMENT 1: DYNAMIC FRICTION (CASE 1)

3.1 Dynamic Friction: Testing Parameters

In the dynamic friction experiment the rate and state friction b-value was changed to assess how it impacts earthquake magnitude distribution, event timing, and total number of events. Injection rate was held constant at 9 kg/s, the experiment ran for 25 years and boundary conditions were no flow. The four rate and state friction b-values tested were 0.011, 0.014, 0.018, and 0.022. These rate and state b-values correspond to a dynamic friction of 0.6270, 0.5579, 0.4658, and 0.3737. Each of these conditions was applied to the four study areas.

3.2 Dynamic Friction: Results

In Figure 4 each of the study areas are plotted to show how cumulative injection volume effected the total number of earthquakes. Figure 5 has the combined results of the four study areas and shows how cumulative injection volume effects number of earthquakes (a) and moment magnitude (b). We observed that as dynamic friction decreased, less cumulative injected volume was needed to cause rupture. With lower dynamic friction, the total number of earthquake generated during the simulation increased. Also with lower dynamic friction the maximum magnitude of the earthquakes increased.

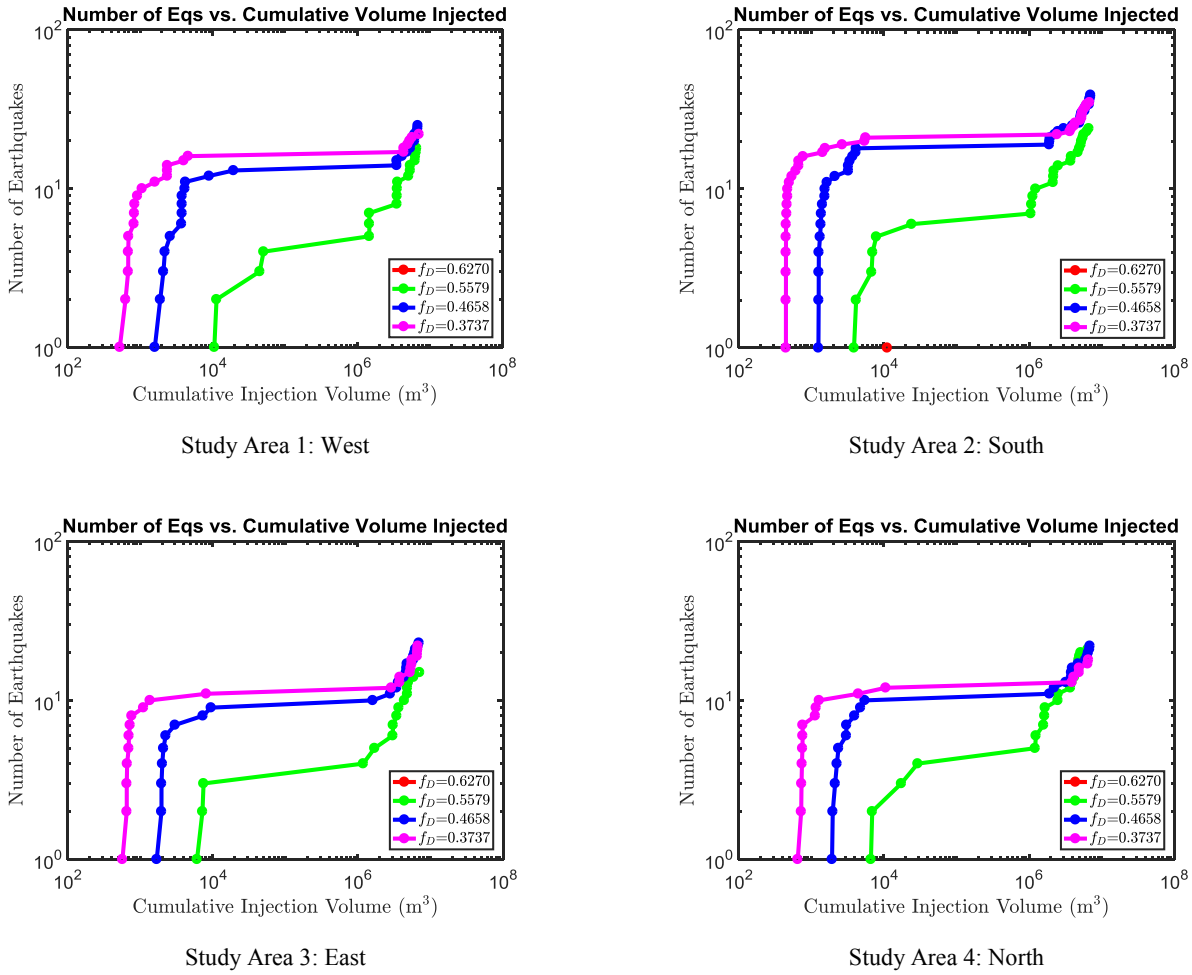

Study Area 1: West

Study Area 2: South

Study Area 3: East

Study Area 4: North

Figure 4: Results from the dynamic friction experiment four study areas displaying the number of earthquakes vs cumulative injection volume.

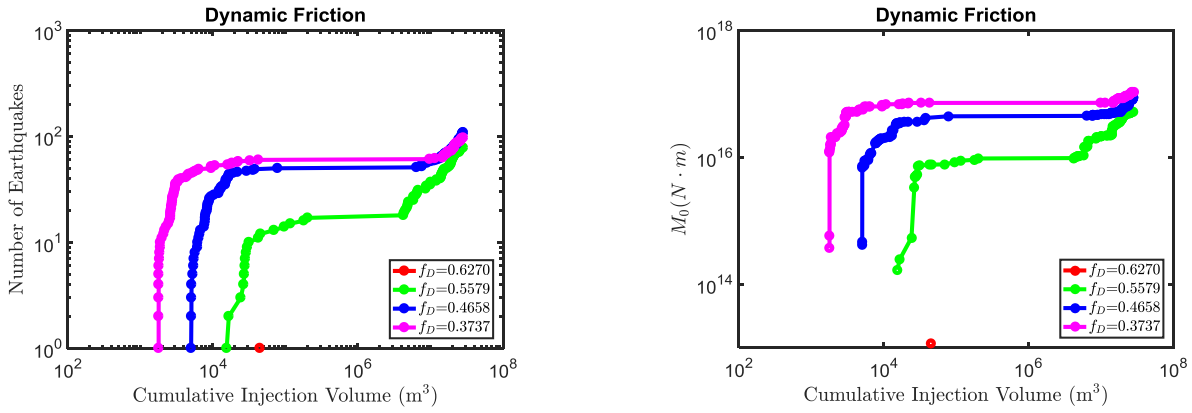

(a) **(b)**

Figure 5: The combined results of the four study areas for the dynamic friction experiment. The left chart (a) illustrates the number of earthquakes vs cumulative injection volume. The right chart (b) shows maximum magnitude vs cumulative injection volume. As dynamic friction decreased earthquake nucleation occurred with less injected volume, total number of earthquakes increase, and maximum magnitude increased.

4. EXPERIMENT 2: INJECTION RATE VARIABLITY (CASE 2)

4.1 Injection Rate Variability: Testing Parameters

The injection rate variability experiment compared two different injection schedules to see how it would affect earthquake frequency-magnitude distribution, event timing, and the total number of events. The first pumping schedule was a constant 9 kg/s injection rate. The second pumping schedule injected at a rate of 18kg/s and cycled between periods of injection and shut-in on a monthly basis. Therefore, the cumulative volume of fluid injected was equal for both scenarios. The experiment ran for 25 years, a rate-and-state friction coefficient of $b = 0.014$ (dynamic friction f_D=0.5579), and boundary conditions were tested for no-flow boundary and fixed-pressure boundary.

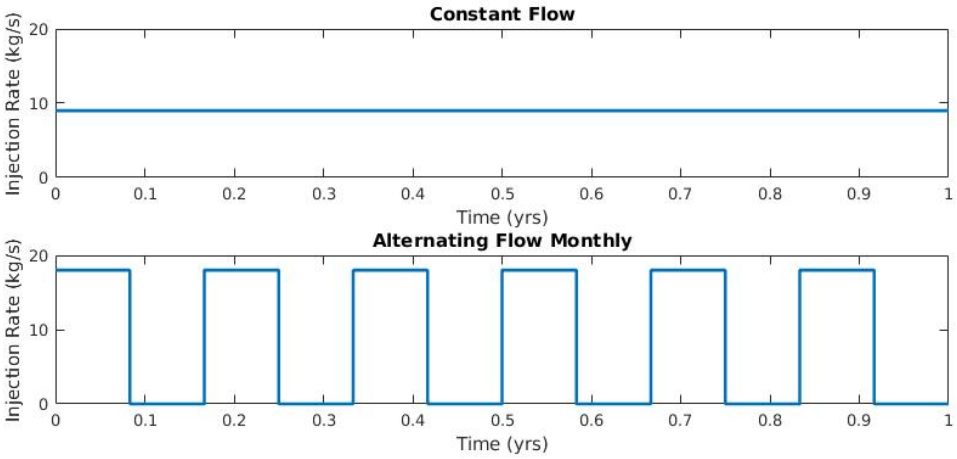

Figure 6: Example for one year of pumping for the constant injection rate (9 kg/s) and alternating monthly flow (18 kg/s). Experiment ran for 25 years.

4.2 Injection Rate Variability: Results

For Case 2, the results of the four study areas were aggregated to form a single catalog. When the fixed-pressure boundary condition was tested all of the earthquakes occurred within the first 37 days of the experiment for both pumping schedules. Although the experiment had ran for a full 25 years earthquakes only occurred during the first 37 days because of the fixed boundary condition. Pressures within the system remained relatively low, therefore, only faults that were nearly at critical stress conditions initially could fail. Earthquake rupture occurred with nearly the same timing at both injection scenarios for the first 30 days. For the higher injection rate scenario of 18kg/s, we observed that the first few earthquakes occurred at nearly exactly the same time as the case with constant injection rate. In Section 5, we discuss why this behavior occurred. Figure 7a shows the number of earthquakes as a function of time. Earthquakes continued to occur during shut in for the 18kg/s monthly case. Figure 7b shows the number of earthquakes as a function of cumulative injection volume. There was a sharp vertical increase for the 18kg/s at higher cumulative injection volume. This was because these earthquakes occurred in a period of shut in for the 18kg/s monthly case.

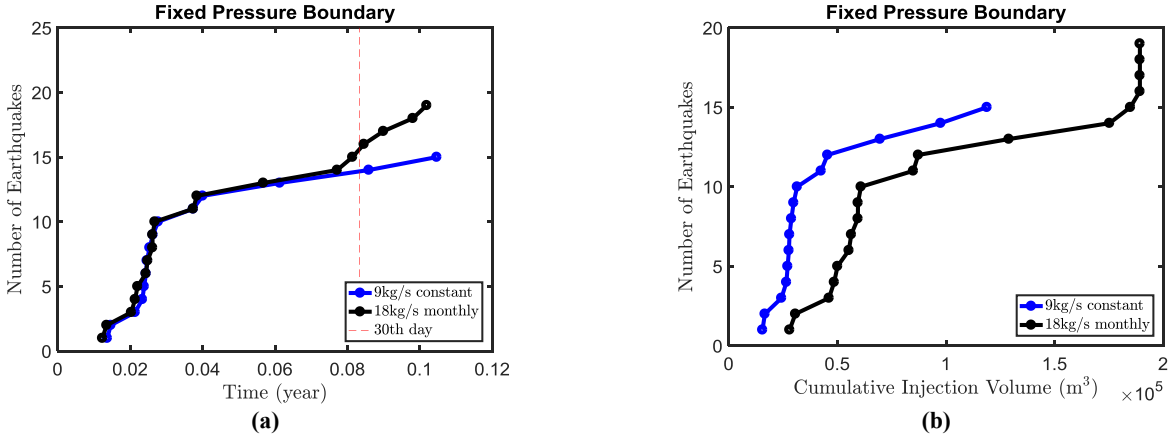

Figure 7: Results for injection rate variability experiment with fixed pressure boundary conditions (Case 2A). The left chart (a) displays the number of earthquakes vs time. The right chart (b) shows the number of earthquake vs. total injection volume.

When the no-flow boundary condition was tested, the results were identical to the first 37 days of the fixed-pressure boundary conditions. The no-flow boundary results differed from those of the fixed-pressure boundary case after the first 37 days. Between 37 days and 65 days, two more events occurred for the 9 kg/s injection rate scenario. There was a period of no seismicity between 65 days and 1360 days. Seismicity after the 1360 days was nearly identical for both pumping schedules.

During the first month, the injection volume was double for the 18kg/s alternating schedule to produce the same number of earthquakes as 9 kg/s continuous schedule. After the first month, the cumulative injection volume and number of earthquakes were nearly the same for both pumping schedules. At the end of the 25 years of the experiment the 9 kg/s continuous pumping produced 78 earthquakes and the 18 kg/s alternating monthly produced 80 earthquakes.

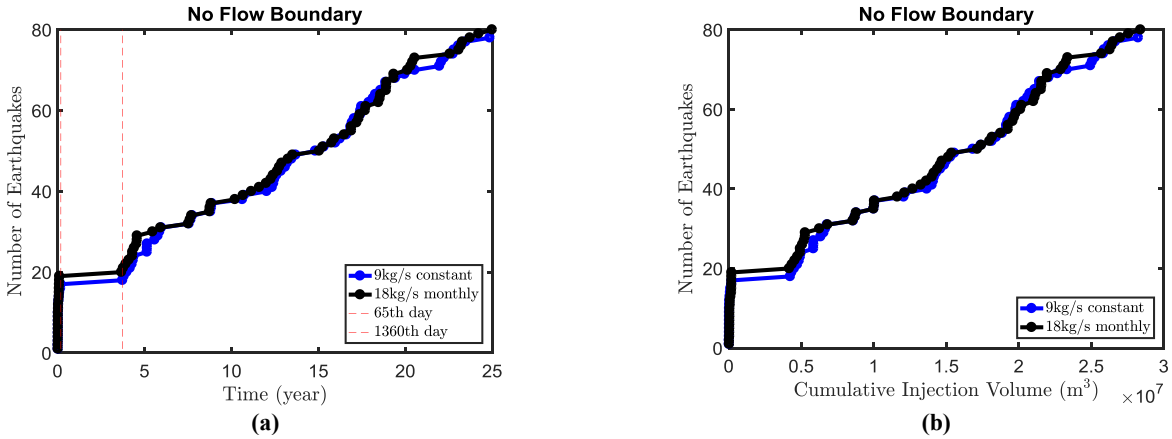

Figure 8: Results for injection rate variability experiment with no flow boundary conditions (Case 2B). The left chart displays the number of earthquakes vs time (a). The right chart shows the number of earthquake vs total injection volume (b).

During the 18 kg/s alternating pumping schedule, the moment magnitude was higher for the first 65 days (first cycle of earthquakes). Between 65 days and 1360 days no earthquakes occurred. After the 1360 days fault failure begins again (second cycle). By the end of the experiment (25 years) the moment magnitude converges the total moment magnitude of the 9 kg/s continuous pumping was $5.223\times10^{16}(N\cdot m)$ and the 18 kg/s alternating monthly moment magnitude was $5.229\times10^{16}(N\cdot m)$.

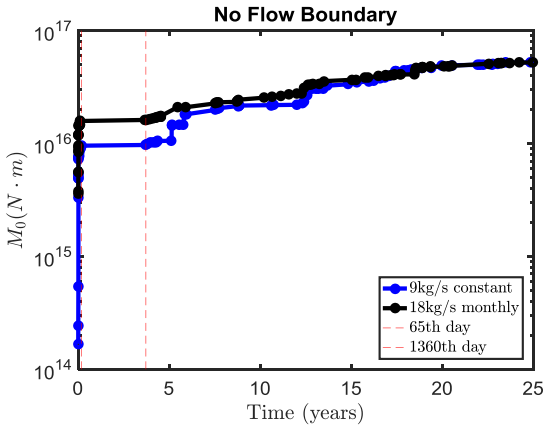

Figure 9: Results for injection rate variability experiment with no flow boundary conditions. Moment magnitude vs total injection volume.

5. DISCUSSION

5.1 Dynamic Friction Experiment

Dynamic friction of faults can be determined by measuring the material properties (b and a) in a laboratory setting. It was found in the simulations that as dynamic friction decreased earthquake nucleation occurred with less injected volume, the total number of earthquakes increased, and the maximum magnitude increased.

In the rate-and-state friction framework, the dynamic friction coefficient can be approximated as:

$$f_D \approx f_0 - (b-a)\ln\left(\frac{V_{\max}}{V_0}\right) \tag{1}$$

Where f_0 is the steady-state friction coefficient at the reference sliding velocity V_0, a controls the magnitude of the direct velocity-strengthening effect, b controls the magnitude of the state evolution effect, and $V_{\max}$ is the sliding velocity during an earthquake rupture. For faults in nature, the maximum sliding velocity is approximately $V_{\max} \approx 1$ m/s.

When dynamic friction is lower, the stress drop is greater. The magnitude of the stress drop influences seismic moment. The stress drop can be calculated as:

$$\Delta\tau = \tau_0 - \bar{\sigma} f_D . \tag{2}$$

The seismic moment depends on the distribution of slip along the fault:

$$M_0 = G \int \delta dA . \tag{3}$$

Assuming a uniform stress drop along a planar fault for a mode-II rupture under plane strain conditions, the Eq. (7) can be calculated as (Pollard and Segall, 1987):

$$M_0 = \pi c^2 H (1-\nu)\Delta\tau \tag{4}$$

In Eqs. (2) through (4), τ_0 is the initial shear stress acting on the fault, $\bar{\sigma}$ is effective stress, δ is shear slip displacement, A is the fault surface area, G is shear modulus, c is half-length of the fault, H is height, and υ is Poisson's ratio.

Dynamic friction controls the stress drop and therefore with lower dynamic friction higher magnitude earthquakes occur. This concept is evident in the modeled earthquakes. This correlation is important when considering the statistical properties of the Gutenberg Richter b-value (frequency-magnitude scaling factor). With lower dynamic friction the Gutenberg Richter b-value decrease.

5.2 Injection Rate Variability

For this experiment two different pumping schedules were being used. The first was a continuous pumping schedule of 9 kg/s the second was a monthly alternating schedule of 18 kg/s and no pumping. Fluid was injected during the first month for both scenarios.

Two different variables controlled earthquake rupture: dimensionless pressure and radius of investigation. As fluid was pumped into to the system it caused the pore pressure to increase and the effective stress to decrease. Each fault had a critical pressure perturbation required to cause shear failure. Dimensionless pressure can be written as:

$$p_D = \frac{2\pi kh}{qB\mu}\left(p_i - p_{\omega f}\right) \tag{5}$$

The radius of investigation equation is a function of time:

$$r_{inv} = C\sqrt{\frac{\kappa t}{\varphi\mu c_t}} \tag{6}$$

where κ is permeability; t is time; ϕ is porosity; μ is viscosity; c_t is total system compressibility; C is a constant; h is thickness; q is productivity rate; B is formation volume factor; p_i is initial reservoir pressure; p_{wf} is well flowing pressure (Horne, 1995).

During the first month of the experiment earthquakes occurred with nearly the same timing for both an injection rate of 9 kg/s and 18kg/s. We recognize that in porous media pressure evolves according to a diffusion equation, so terms such as pressure front are generally inappropriate. However, in the context of induced seismicity, we can define the pressure front as the location at which the pressure has exceeded the critical pressure required to cause shear failure on a given fault. The speed in which the pressure front moved in the system is a function controlled by the radius of investigation (see Eq. (6)). The radius of investigation is a function of time and the

hydraulic properties of the formation, but it is not a function of injection rate. Figure 10 illustrates how the radius of investigation was moving outwards with time. Even though the two pumping routines were injecting at different rates, the movement of the pressure front at a higher injection rate is the same as the movement of the pressure front at the lower injection rate. Therefore, the earthquakes ruptures had the same timing because the pressure front of the two scenarios moved with the same timing and the faults were near failure so the lower dimensionless pressure (due to lower injection rate) was high enough to cause failure.

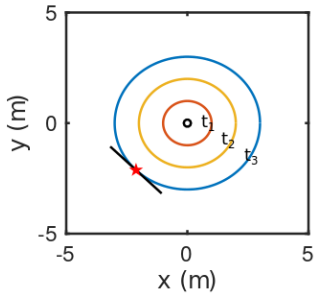

Figure 10: The radius of investigation was controlled by time not by injection rate. Therefore, at both a higher injection rate and lower injection rate the radius of investigation was equivalent.

After the first month, injection was switched off for the variable injection rate scenario. Even though no injection occurred, seismicity continued. More earthquakes occurred for the alternating case than for the continuous pumping scenario. This could be because the pressure front continued to move outward even when injection was stopped. The dimensionless pressure was higher for the alternating pumping case, therefore, faults reached the critical pressure and failure, whereas, for the lower pumping rate the dimensionless pressure was lower, and therefore, faults did not yet reach failure.

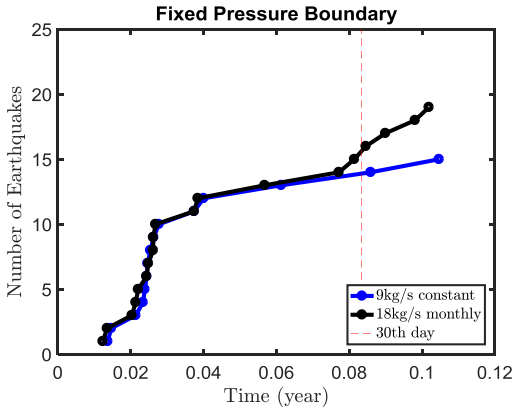

Figure 11: Results for injection rate variability experiment with fixed pressure boundary conditions. The red line indicates the end 30th day.

There is a gap in seismicity between 65 days and 1360 days. The faults that were near failure were able to rupture early in the experiment with low pressure. More injection needed to occur to build pressure so faults would begin to fail again.

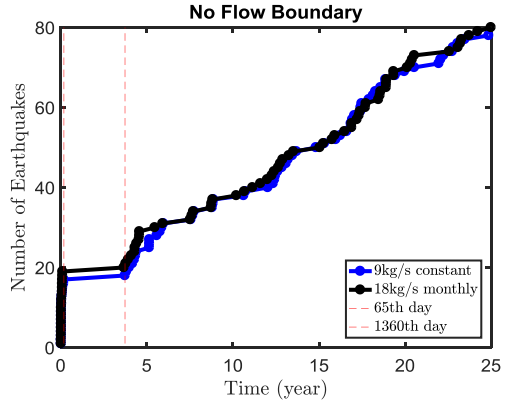

Figure 12: Results for injection rate variability experiment with no flow boundary. The time between the 2 red lines displays a gap in seismicity between 65 days and 1360 days.

For the second cycle of earthquakes (after 1360 days) the event timing was similar. The higher injection pumping schedule varied from 18kg/s to shut-in, whereas, the lower injection schedule was 9 kg/s constantly. The number of earthquakes that occurred was similar because the total injection volume in the system was the same for both pumping routines; therefore, the average pressure in the system was similar in both cases.

For the variable injection rate experiment, the same cumulative volume was injected for both pumping scenarios after 25 years. Having a continuous pumping schedule of 9kg/s and alternating monthly between pumping at 18 kg/s and shut-in had little effect on the total number of earthquakes and total moment magnitude at the end of the 25 years. However, more studies should be performed to see how different frequencies, such as longer periods of shut in, would effect on the total number of earthquakes and total moment magnitude before a conclusion can be made.

6. CONCLUSION

We observed that as dynamic friction decreased, smaller cumulative injected volume was needed to cause rupture. With lower dynamic friction, the total number of earthquakes generated during the simulation increased. In addition, with lower dynamic friction the maximum magnitude of the earthquakes increased. The correlation between dynamic friction and magnitudes can be explained because of the influence of dynamic friction on the stress drop. Seismic moment scales linearly with stress drop, therefore earthquakes with similar rupture patch sizes but lower dynamic friction (i.e., larger stress drop) have larger magnitudes.

During the first month of injection, the total injection volume of higher injection rate of 18kg/s was double that of the lower injection rate of 9kg/s. The events occurred at exactly double the cumulative injection volume, suggesting that the 'pressure front' was moving at exactly the same speed in both cases, regardless of the injection rate at the well. This implies that the magnitude of the pressure threshold required to cause slip was negligible, so the faults that slipped first must have been almost exactly critically stressed.

After the first month, dimensionless pressure controlled the rate of earthquakes. For the alternating case, the injection well was shut in during the second month so that no injection was occurring; yet seismicity was higher than the continuous pumping scenario. The pressure front continued to move outward even when the well was shut in, ultimately exceeding the critical pressure of the faults. The lower continuous pumping rate dimensionless pressure was lower during this time, therefore, the faults had not yet reached failure. Because earthquakes only occurred with the first 37 days of the experiment for Case 2A this higher dimensionless pressure caused the alternating injection rate scenario to have more earthquakes occur than the continuous pumping scenario.

In Case 2B pressures continued to build due to the no flow boundary, and earthquakes continued to occur for the full 25 years. There is a gap in seismicity between 65 days and 1360 days. This behavior occurred because faults that were nearly critically stressed before injection failed at relatively low pressures. In the no flow boundary condition (Case 2B), pressure continued to build, which caused earthquakes start to occur again once critical stress levels on the faults were reached. Following 1360 days, the number of earthquakes in both pumping schedules was nearly identical.

For Case 2A (fixed pressure boundary condition) earthquakes only occurred during the first 37 days. The alternating monthly between 18 kg/s and shut in caused a slight increase in the total number of earthquakes and total moment magnitude compared to the 9 kg/s continuous flow schedule. For Case 2B (no flow boundary conditions), the testing scenarios of 9 kg/s continuous and alternating monthly between 18 kg/s and shut did not prove to cause significant change in total number of earthquakes and total moment magnitude by the end of the 25 years. Therefore, for this testing scenario the injection rate variability had little to no effect on the Gutenberg-Richter a-value (seismicity rate) and b-value (frequency-magnitude scaling factor).

REFERENCES

Baker, T.: Wells located within Expanded Areas of Interest for Triggered Seismicity. Oklahoma Corporation Commission (2016).

Ellsworth, W.: Injection-induced earthquakes, *Science*, 341(6142), (2013), doi: 10.1126/science.1225942.

Holland, A. A.: Preliminary Fault Map of Oklahoma, Oklahoma Geological Survey Open File Report, OF3-2015 (2015).

Horne, R. N.: Dimensionless Variables. *Modern Well Test Analysis: A Computer-Aided Approach***,** (1995),10-11

Majer E. L., Baria R., Stark M., Oates S., Bommer J., Smith B., Asanuma H.: Induced seismicity associated with Enhanced Geothermal Systems, *Geothermics*, **36** (3), 185–222, (2007), http://dx.doi.org/10.1016/j.geothermics.2007.03.003.

McClure, M.W.: Modeling and Characterization of Hydraulic Stimulation and Induced Seismicity in Geothermal and Shale Gas Reservoirs, PhD thesis, Stanford University, Stanford, California, USA (2012).

McGarr, A., Bekins, B., Burkardt, N., Dewey, J., Earle, P., Ellsworth, W., Ge, S., Hickman, S., Holland, A., Majer E., Rubinstein, J.,& Sheehan, A.: Coping with earthquakes induced by fluid injection. *Science*, **347**(6224), (2015), 830-831.

McGarr, A.: Maximum magnitude earthquakes induced by fluid injection, *Journal of Geophysical Research: Solid Earth*, 119, 1008–1019, (2014) doi:10.1002/2013JB010597.

Norbeck, J.H.: Hydromechanical and frictional faulting behavior of fluid-injection-induced earthquakes, PhD thesis, Stanford University, Stanford, California, USA (2016).

Norbeck, J.H., and Horne, R.N.: Evidence for a transient hydromechanical and frictional faulting response during the 2011 Mw 5.6 Prague, Oklahoma earthquake sequence, *Journal of Geophysical Research: Solid Earth*, **121**(12), (2016), 8688-8705, doi: 10.1002/2016JB013148.

Norbeck, J.H., McClure, M.W., Lo, J.W., and Horne, R.N.: Simulation of hydraulic fracturing and shear stimulation within an embedded fracture modeling framework, *Computational Geosciences*, **20**(1), (2016), 1-18, doi: 10.1007/s10596-015-9543-2.

Petersen, M. D., Mueller, C. S., Moschetti, M. P., Hoover, S. M., Llenos, A. L., Ellsworth, W. L., Michael, A. J., Rubinstein, J. L., McGarr, A. F., & Rukstales, K. S.: 2016 One-Year Seismic Hazard Forecast for the Central and Eastern United States from Induced and Natural Earthquakes (No. 2016-1035). US Geological Survey. (2016)

Pollard, D.D., and Segall, P.: Theoretical displacements and stresses near fractures in rock: with applications to faults, joints, veins, dikes, and solution surfaces, in *Fracture Mechanics of Rock,* edited by B. Atkinson, Academic Press Inc., London, (1987).

Shammas, N. K., Wang, L. K., & Sever, C. W.: Proper Deep-Well Waste Disposal for Water Resources Protection. *In Natural Resources and Control Processes*, Springer International Publishing, (2016), 119-185

Walsh, F.R., and Zoback, M.D.: Oklahoma's recent earthquakes and saltwater disposal, *Science Advances*, 1(5), (2015), e1500195, doi:101126/sciadv.1500195.

Walsh, F.R., and Zoback, M.D.: Probabilistic assessment of potential fault slip related to injection-induced earthquakes, *Geology,* **44**(12), (2016), 1-4, doi: 10.1130/G38275.1.